



HAL
open science

Design of acoustic absorbing metasurfaces using a data-driven approach

Hamza Baali, Mahmoud Addouche, Abdesselam Bouzerdoum, Abdelkrim Khelif

► **To cite this version:**

Hamza Baali, Mahmoud Addouche, Abdesselam Bouzerdoum, Abdelkrim Khelif. Design of acoustic absorbing metasurfaces using a data-driven approach. *Communications Materials*, 2023, 4 (1), pp.40. 10.1038/s43246-023-00369-0 . hal-04288333

HAL Id: hal-04288333

<https://hal.science/hal-04288333>

Submitted on 16 Nov 2023

HAL is a multi-disciplinary open access archive for the deposit and dissemination of scientific research documents, whether they are published or not. The documents may come from teaching and research institutions in France or abroad, or from public or private research centers.

L'archive ouverte pluridisciplinaire **HAL**, est destinée au dépôt et à la diffusion de documents scientifiques de niveau recherche, publiés ou non, émanant des établissements d'enseignement et de recherche français ou étrangers, des laboratoires publics ou privés.

Design of Acoustic Absorbing Metasurfaces Using a Data-Driven Approach

Hamza Baali¹, Mahmoud Addouche², Abdesselam Bouzerdoum^{1,3}, Abdelkrim Khelif²

¹Division of Information and Computing Technology, College of Science and Engineering, Hamad Bin Khalifa University, Doha, Qatar

²Institut FEMTO-ST, CNRS, Université de Bourgogne Franche-Comté 15B Avenue des Montboucons, CEDEX, F-25030 Besançon, France

³School of Electrical, Computer and Telecommunications Engineering, University of Wollongong, Wollongong, Australia

Abstract

The design of new acoustic metasurfaces with desirable properties is challenging due to their artificial nature and the large search space of physical and geometrical parameters. This paper presents an efficient two-stage data-driven approach for analyzing and designing membrane-type metasurface absorbers with desirable characteristics. In the first stage, a forward model consisting of a neural network is trained to map an input, comprising the membrane parameters, to the observed sound absorption spectrum. Then, in the second stage, the learned forward model is inverted to infer the input parameters that produce the desired absorption response. The metasurface membrane parameters, which serve as input to the neural network, are estimated by minimizing a loss function between the desired absorption profile and the output of the learned forward model. Finally, two devices are fabricated using the estimated membrane parameters. The measured acoustic absorption responses of the fabricated devices show a very close agreement with the desired responses.

Keywords: Acoustic metasurfaces, Deep learning, Neural network, Inverse design, Sound absorption

1. Introduction

The first successful fabrication of metamaterials by Smith et al. [1] two decades ago revolutionized the conventional view of electromagnetic and acoustic wave propagation. It opened the doors to engineer new materials with variable properties not found in natural materials [2-4]. In essence, metamaterials are artificially structured composite materials characterized by built-in locally resonant structures (LRS). These structures restrain/localize strongly oscillating acoustic or electromagnetic fields in the bulk of the structured materials or on the surface, in the case of metasurfaces, to specific frequencies. The presence of these LRSs allows the control and modulation of incident waves at subwavelength frequency.

Over the past two decades, various metamaterials and metasurfaces have been developed with new acoustic properties: acoustic cloaking [5-7], complete sound reflection and transmission [8-10], complete sound absorption [11-17], and wavefront tailoring [18]. This study concerns sound absorption applications in which conventional approaches rely on materials with limited acoustic performance, such as glass, wool, and perforated panels backed by air cavities [19-21]. These conventional absorbers are characterized by thicknesses having wavelengths in the audible range, which require large mass, limiting the scope of their applications and efficiency. One innovative way to overcome this limitation is using decorated metasurface membranes that can achieve nearly total absorption at low frequency with dimensions much smaller than the wavelength of incident sound waves.

Until recently, however, **the analysis of metasurface-based absorbers** was primarily based on numerical simulations of physics-based models using either Finite Element methods (FEM) via solvers such as the COMSOL Multiphysics or through finite-difference time-domain (FDTD) methods. The former approach can model complex scenarios and geometries at the cost of slow simulation. This limitation adds to the inconvenience of the black-box nature of the calculations of these commercial packages, which can only

provide a posteriori explanation. By contrast, the latter approach is appropriate only for scenarios of low to moderate complexity [22]. The fast development of deep learning (DL) techniques in the last decade coupled with the increasing computing power and the growth in data availability has made them a feasible surrogate of FEM for the analysis of acoustic wave systems, both in the time and in the frequency domains [23-26]. DL is based on universal function approximators leveraged to specific problems through learning from data. This data is usually generated from high-fidelity numerical simulations or through physical experiments. One significant advantage of these data-driven approaches is that they do not require knowledge of the governing equations of the system and are much faster than physics-based simulations.

The inverse design of metasurfaces is a high-dimensional non-convex optimization problem that seeks to find optimal metamaterial parameters to achieve a desired behavior. Conventional approaches rely either on nonlinear optimization approaches, such as genetic algorithms (GAs), or heuristic methods. Nonlinear optimization approaches are computationally expensive due to repeated sampling and are susceptible to convergence failure. On the other hand, heuristic approaches cannot systematically search a large design space as they rely heavily on trial and error and extensive experimentation [27]. The emergence of new data-driven approaches in recent years has led to a shift in the design paradigm of metamaterials [28-30].

The idea of inverse design using data-driven approaches was initially proposed to analyze neural network architectures [31-32]. The adaptive control community used these approaches to circumvent the limitations and unfeasibility of direct inverse modeling of dynamical systems, which is an ill-posed problem in the Hadamard sense [33]. These approaches have recently gained significant attention in electromagnetic and acoustic metamaterials [34-36]. Popular inverse design approaches include iterative gradient-based and indirect inversion using tandem configuration. In this configuration, a particular inverse solution of an already trained network is connected in series with another network to accomplish an auto-association task (learning an identity mapping across the composite network). In this setup, the forward model allocates one output to each frequency sampling point in the absorption spectrum which leads to significant number of free parameters [37-38]. Other alternative inversion approaches include direct inverse design and global optimization algorithms enabled by generative neural network approaches and NN inversion through constrained optimization formulations [39-41].

This paper deploys a data-driven approach for forward modeling and inverse design of membrane-based metasurface absorbers. By observing the metasurface parameters (input) and the sound absorption spectrum (output), a forward neural network (NN) model learns a nonlinear function that maps inputs to outputs through the minimization of the prediction error. Once trained, the NN model reduces the high computational demands of conventional forward physics simulations into a single forward pass. We demonstrate the effectiveness of the learned model by producing accurate outputs from parameters that were not used in the training phase. The learned model is then inverted to estimate the membrane parameters (input) that yield the desired response. The inversion is cast as an optimization problem by minimizing the error between the desired response and the predicted output. The objective is to find the set of membrane parameters that minimize the prediction error over a set of frequencies while keeping the forward model parameters (weights and biases) fixed. The proposed inversion approach provides flexibility in optimization, enabling consideration of only the desired absorption at a specific frequency or range of frequencies of interest. In contrast, the tandem architecture does not allow for such specificity. Furthermore, since the inverse problem is purely an optimization-based approach, there is more flexibility to vary the objective function or introduce appropriate constraints, e.g., adding a regularization term without having recourse to retraining of the entire model. Such flexibility is not possible with the tandem configuration.

The rest of the paper is organized as follows. Section 2 presents an exposition of the mathematics of the NN based forward model and a formulation of the inverse design as an optimization problem. Section 3 describes the generation of the training dataset using FEM. Section 4 discusses the training of the forward NN and evaluates its performance against the FEM model. The results of NN inversion to determine the membrane parameters for a given sound absorption spectrum are discussed in Section 5. Finally, Section 6 presents some concluding remarks.

2. Forward and inverse modeling

This section describes the forward and inverse models adopted in this study. First, a forward model is learned by training a neural network to predict the sound absorption spectrum, using the membrane's physical parameters and the frequency as input. Second, an inverse model is learned indirectly using the forward model to find the membrane parameters which produce a desired sound absorption profile.

2.1 The forward model

An L layer feedforward neural network, with N inputs ($\mathbf{x} \in \mathbb{R}^N$) and one output ($y \in \mathbb{R}$), is trained to approximate the physical model, $\Phi(\mathbf{x})$, that generates the training data. The network realizes a composite function, which can be expressed as:

$$\mathbf{F}(\mathbf{x}; \boldsymbol{\theta}) = \mathbf{F}_{L-1}(\mathbf{F}_{L-2}(\cdots \mathbf{F}_l \cdots (\mathbf{F}_1(\mathbf{x}))), \quad (1)$$

where $\boldsymbol{\theta}$ denotes the network free parameters. The expression (1) means that the output \mathbf{y}_l of each elementary function $\mathbf{F}_l: \mathbb{R}^{N_{l-1}} \rightarrow \mathbb{R}^{N_l}$ becomes the input of the following function. Each of these elementary functions comprises two parts, a linear affine transformation ($\mathbf{W}_l \mathbf{y}_{l-1} + \mathbf{b}_l$) and a nonlinear elementwise activation function $\mathbf{H}(\cdot)$. We can write \mathbf{y}_l in the form:

$$\begin{aligned} \mathbf{y}_1 &= \mathbf{F}_1(\mathbf{y}_0) = \mathbf{H}(\mathbf{W}_1 \mathbf{y}_0 + \mathbf{b}_1), \quad \mathbf{y}_0 = \mathbf{x}, \\ \mathbf{y}_l &= \mathbf{F}_l(\mathbf{y}_{l-1}) = \mathbf{H}(\mathbf{W}_l \mathbf{y}_{l-1} + \mathbf{b}_l), \quad l = 2, \cdots, L-1 \end{aligned} \quad (2)$$

The parameters $\boldsymbol{\theta}_l = [\mathbf{b}_l \ \mathbf{W}_l]$ represent the network parameters including the weights ($\mathbf{W}_l \in \mathbb{R}^{N_{l-1} \times N_l}$) and biases ($\mathbf{b}_l \in \mathbb{R}^{N_l}$). Popular nonlinear elementwise functions $\mathbf{H}(\cdot)$ include the sigmoid, hyperbolic tangent and the ReLU activation functions.

The training involves adjusting the network parameters to minimize a loss function that measures the discrepancy between the network output $y = y_{L-1} = \mathbf{F}(\mathbf{x}; \boldsymbol{\theta})$ and the desired (ground-truth) output $r = \Phi(\mathbf{x})$ when subjected to same input, as summarized in Fig. 1.

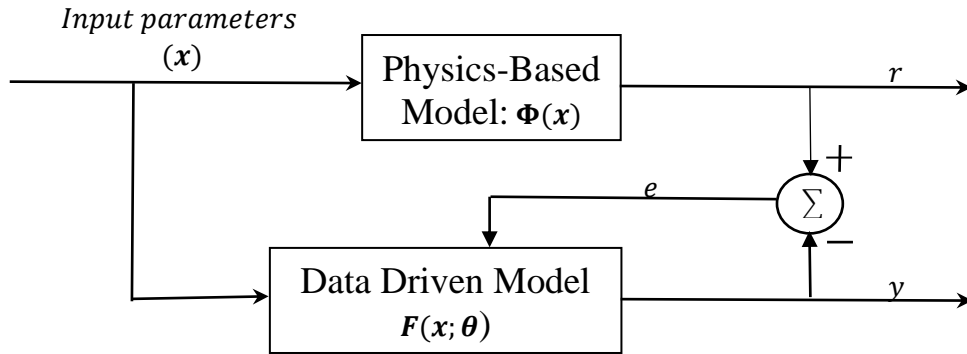


Fig. 1. A block diagram of the forward model learning from the inputs and outputs of the physics-based model. The same input \mathbf{x} is applied to the system $\Phi(\mathbf{x})$ and to the network $\mathbf{F}(\mathbf{x}; \boldsymbol{\theta})$. The desired network weights are found by minimizing a loss function of the prediction error $e = (r - y)$.

Given a training dataset D of P typical input and desired output samples $\{\mathbf{x}^{(i)}, r^{(i)}\}_{i=1}^P$, where $r^{(i)} = \Phi(\mathbf{x}^{(i)})$. The network input vector $\mathbf{x}^{(i)} = [x_1^{(i)}, x_2^{(i)}, \cdots, x_N^{(i)}]^T$ comprises the frequency $f^{(i)} = x_1^{(i)}$ and the

membrane parameters $\mathbf{x}_{2:N}^{(i)} = [x_2^{(i)}, \dots, x_N^{(i)}]^T$. The task of training a network is to find the best set of parameters (i.e., weights) $\boldsymbol{\theta}^*$ that minimize the mean sum of squares of the network errors over the training set:

$$g(\boldsymbol{\theta}) = \frac{1}{P} \sum_{i=1}^P (r^{(i)} - y^{(i)})^2 = \frac{1}{P} \sum_{i=1}^P (r^{(i)} - \mathbf{F}(\mathbf{x}^{(i)}; \boldsymbol{\theta}))^2 \quad (3)$$

There exist several optimization techniques to minimize $g(\boldsymbol{\theta})$, such as the Gradient-descent and its variants, Newton's method, and Levenburg-Marquard algorithm. Most Gradient-descent-like methods involve recursive calculation of the partial derivatives of the loss function g with respect to the network parameters $\boldsymbol{\theta}$ and then use of these derivatives to update the network parameters in the direction that reduces the overall loss g , i.e., the negative gradient direction. The standard gradient-descent update rule for the weights has the form:

$$\boldsymbol{\theta}^{(k+1)} = \boldsymbol{\theta}^{(k)} - \eta \nabla_{\boldsymbol{\theta}} g(\boldsymbol{\theta}^{(k)}), \quad (4)$$

where $(0 < \eta < 1)$ is the learning rate and $\nabla_{\boldsymbol{\theta}}$ is the gradient operator with respect to $\boldsymbol{\theta}$. In practice, the partial derivative forming the gradient $\nabla_{\boldsymbol{\theta}}$ are calculated using the backpropagation algorithm, an efficient algorithm that exploits the composite and the differentiability nature of \mathbf{F} to compute the derivatives in reverse mode according to the chain rule.

2.2 The inverse model

In this part, we aim to estimate the metamaterial parameters $\mathbf{x}_{2:N}$ for which the earlier learned forward model $\mathbf{F}(\mathbf{x}; \boldsymbol{\theta}^*)$ approximates a 'fictitious' desired sound absorption profile ($\mathbf{r}^d = [r_1, r_2, \dots, r_m, \dots, r_M]^T$) specified by the user, where r_m is the desired absorption coefficient at frequency f_m .

Let $\mathbf{y} = [y_1, y_2, \dots, y_M]^T$ be the actual network output sound absorption profile as function of frequency when its inputs are $\{[f_m, \mathbf{x}_{2:N}]^T\}_{m=1}^{m=M}$. The problem of inverting a neural network model can be then cast as an optimization problem over the network inputs $\mathbf{x}_{2:N}$:

$$\min_{\mathbf{x}_{2:N}} E(\mathbf{x}) = \min_{\mathbf{x}_{2:N}} \|\mathbf{r}^d - \mathbf{y}(\mathbf{x})\|^2 = \min_{\mathbf{x}_{2:N}} \sum_{m=1}^M \|r_m - \mathbf{F}([f_m, \mathbf{x}_{2:N}]^T; \boldsymbol{\theta}^*)\|^2 \quad (5)$$

An efficient way to solve (5) uses gradient-based optimization whereby the gradient $\nabla_{\mathbf{x}}$ with respect to (w.r.t.) the network input elements x_2, x_3, \dots, x_N are calculated using a variant of the backpropagation algorithm similar to the one used for the training of forward model. The partial derivative of $E(\mathbf{x})$ w.r.t. x_i ($i = 2, \dots, N$) is given by

$$\frac{\partial E(\mathbf{x})}{\partial x_i} = \frac{\partial \|\mathbf{r}^d - \mathbf{F}(\mathbf{x}, \boldsymbol{\theta}^*)\|^2}{\partial x_i} = 2 \left(\mathbf{r}^d - \mathbf{F}(\mathbf{x}, \boldsymbol{\theta}^*) \right) \frac{\partial \mathbf{F}(\mathbf{x}, \boldsymbol{\theta}^*)}{\partial x_i}, \quad i = 2, 3, \dots, N. \quad (6)$$

Since the first elements of \mathbf{x} is the frequency f_m , it is not included in the optimization search for parameters. The input update rule adjusts iteratively the remaining elements $\mathbf{x}_{2:N}$ to minimize the difference between the desired outputs r_m and the actual network outputs $y_m = \mathbf{F}([f_m, \mathbf{x}_{2:N}]^T, \boldsymbol{\theta}^*)$ such that:

$$\mathbf{x}_{2:N}^{(k+1)} = \mathbf{x}_{2:N}^{(k)} - \eta \nabla_{\mathbf{x}} E(\mathbf{x}_{2:N}^{(k)}) \quad (7)$$

Fig. 2 summarizes the computation of the gradient $\nabla_{\mathbf{x}}$ using a variant of the backpropagation algorithm, where the network inputs are adjusted instead of its parameters which are held constants.

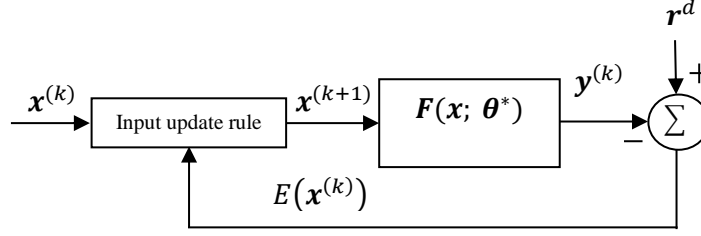


Fig. 2. Iterative inversion of the forward model

The iterative network inversion algorithm can be summarized by the following steps:

Step1: At iteration $k = 0$ assume random values for the of the membrane parameters within their respective ranges $\mathbf{x}_{2:N}^{(k)}$.

Step2: Compute the outputs of the previously trained network for all the frequencies f_m :

$$\mathbf{y}_m^{(k)} = \mathbf{F} \left([f_m, \mathbf{x}_{2:N}^{(k)}]^T, \boldsymbol{\theta}^* \right), m = 1: M .$$

Step3: Compute the sum-squared error: $\mathbf{E}(\mathbf{x}^{(k)}) = \|\mathbf{r}^d - \mathbf{y}^{(k)}\|^2$

Step4: Compute the gradient of $\mathbf{E}(\mathbf{x}^{(k)})$ with respect to $\mathbf{x}_{2:N}^{(k)}$ and update $\mathbf{x}_{2:N}$:

$$\mathbf{x}_{2:N}^{(k+1)} = \mathbf{x}_{2:N}^{(k)} - \eta \nabla_{\mathbf{x}} \mathbf{E} \left(\mathbf{x}_{2:N}^{(k)} \right),$$

Step5: Go to Step 2 and repeat until $\mathbf{E}(\mathbf{x}^{(k)}) < \text{Threshold}$ or $k = k_{max}$

3. Generation of training data

The first step in the process of constructing a forward data driven model consists of generating a representative dataset with known ground-truth that captures different characteristics of the membrane-type acoustic metasurface under investigation. To this end, we generated a realistic dataset D of sound absorption responses for a range of membrane geometric parameter values using numerical simulations. The independent model parameters considered in this study consist of the membrane radius ($a \in [20, 60]$ mm), thickness ($h \in [0.01, 0.5]$ mm) and cavity depth ($e_c \in [1, 40]$ mm). The focus on geometrical parameters is justified by the strong dependence of the acoustic response on membrane geometry. The elastic constants of the material **were selected from COMSOL material library as a stainless steel and** are considered to be fixed including the Young's modulus ($E = 2 \cdot 10^{11}$ Pa), mass density ($\rho = 7850$ kg/m³), Poisson's ratio ($\nu = 0.27$) and effective loss coefficient ($\xi = 0.0613$). The independent parameters are drawn randomly from uniform distributions within their respective ranges.

The FE software COMSOL was used to calculate the acoustic wave reflections in an environment that mimics measurements in an impedance tube according to the ISO 10534-2 protocol. The cylindrical membrane assumed to be backed by an air cavity and clamped in a tube with a square outer section and circular inner hollow section. The acoustical behavior of the membrane is investigated inside a rectangular impedance tube of inner width equals to the outer width of the clamping cube. A unit pressure is applied on the opposite side of the membrane to serve as a normal incidence excitation. The acoustic pressure

interacts with the elastic vibration mode of the membrane inducing sound losses through the visco-thermal effect modeled as an absorbed thin layer attached to the membrane. The simulation configuration is shown in Fig. 3. For each combination of the independent parameters, the normal sound absorption coefficient was recorded for the frequency range 1 to 3000 Hz in 3 Hz increments.

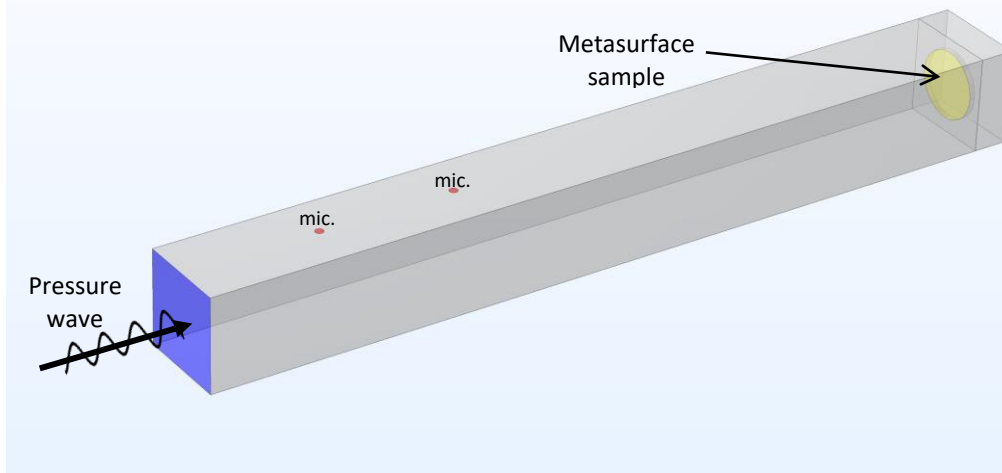


Fig.3. Schematic of the impedance tube configuration

4. Forward model Network architecture

The aim is to train a feedforward neural network to approximate the physics-based membrane model using the training inputs and corresponding targets. The selection of the network topology in terms of number of layers and neurons at each hidden layer is usually found with several trial-and-error training runs. Larger networks can create more complex functions with the risk of overfitting. i.e., small error on the training set and large error on unseen data. Preventing overfitting can be achieved either through regularization, early stopping or by increasing the size of the training set. In this study, the network size was kept large enough to provide a good fit while the size of the training set was increased to avoid overfitting. A neural network with 5 hidden layers and out output (4-24-16-8-4-1) was trained using 50 million data points (100 thousand absorption profiles each contains 500 frequencies). The actual network inputs comprise the membrane radius a , thickness h , cavity depth e_c , and frequency (f). The desired output is the normal absorption coefficient (α) at the frequency f . Prior to training, the data is partitioned into three subsets training, validation, and test sets, with ratios 70 %, 15 %, and 15 %, respectively. All hidden layers use the standard logistic sigmoid activation function, while the output neuron uses a linear activation function. The network was trained using the Levenberg-Marquardt algorithm, which is characterized by an efficient update rule that varies between the gradient descent (Section 2) and the Gauss-Newton method.

Fig.4 shows the plots of the mean squared error (*mse*) loss as a function of the number of training epochs for the training and validation sets. The training and validation errors exhibit similar characteristic, a decreasing function of the number of epochs. The model achieves the lowest validation *mse* of 0.0004 at epoch 556. The agreement between the actual and predicted values is further evaluated statistically through Pearson's correlation coefficient (R) between the model output relative to FEM's desired output. The model performed well with a correlation coefficient of over 0.98.

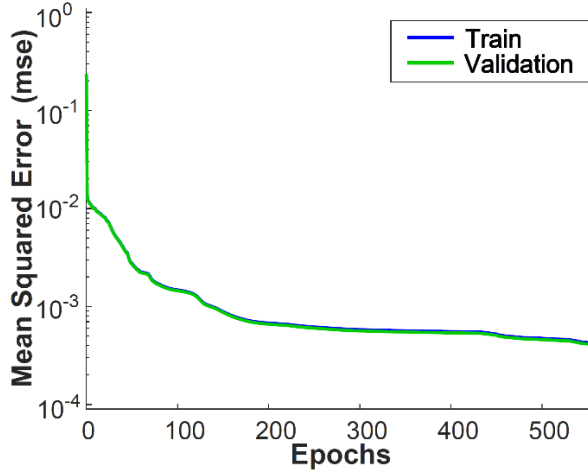


Fig. 4. Mean square error loss function of the training and validation sets as a function of training epochs.

Fig.5 illustrates the network response as a function of frequency for four different sets of input parameters chosen from the test set, except for Fig.5 (d) whose parameters are chosen outside the range of the training parameters. The curves are produced by fixing the physical parameters (a , h , and e_c) and varying the input frequency. The sound absorption curves generated based on the learned model show high fidelity with those based on the FEM simulation across different spectral patterns. Figs.5 (a) and (b) show resonator responses with one and two prominent peaks, respectively. Fig. 5(c) is a broadband absorber with a relative bandwidth of 15 % for an absorption coefficient $\alpha = 0.8$ at the frequency $f = 1165$ Hz.

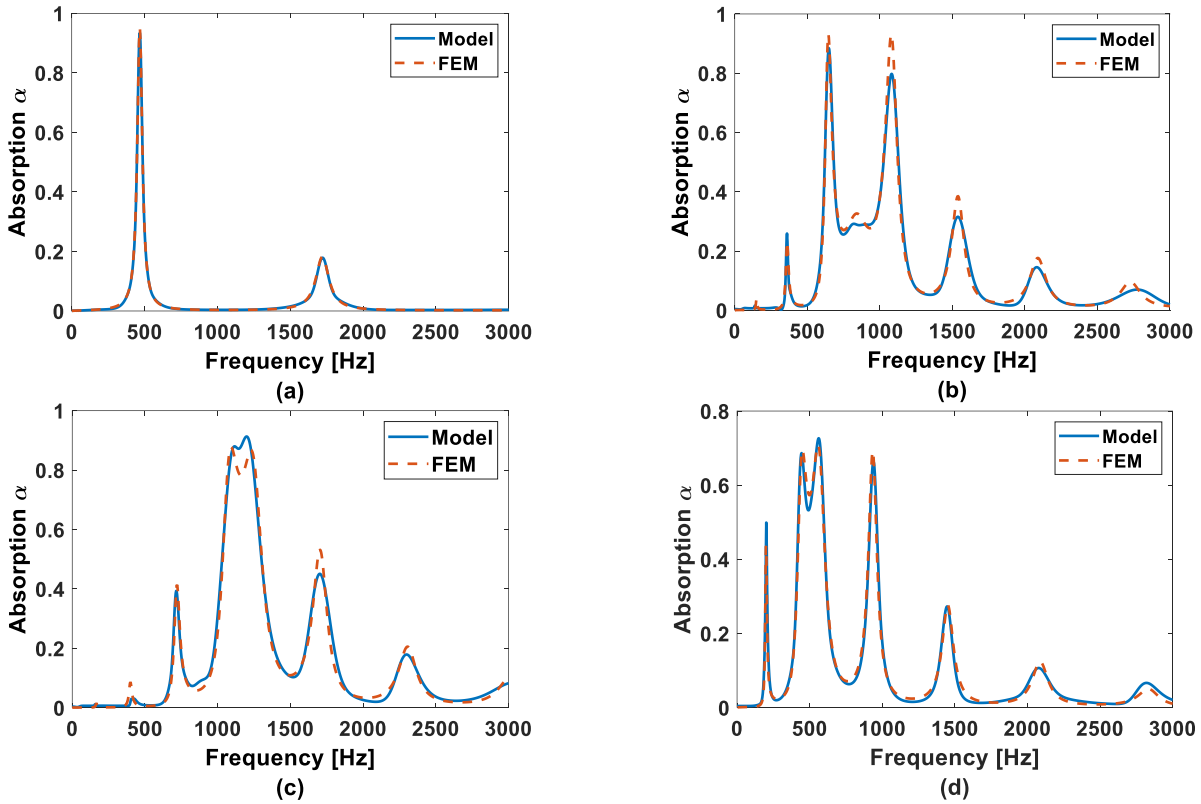


Fig. 5. The model predicted absorption spectrum (blue) and the COMSOL simulated FEM response (red) for four different sets of parameters {radius, thickness, depth}: (a) {45.5, 0.37, 27.5} mm, (b) {33.4, 0.02, 26.5} mm, (c) {45, 0.04, 7.5} mm, and (d) {32, 0.025, 54} mm.

The ability of the model to generalize beyond the range of the training parameters is also evaluated by generating the broadband spectrum of Fig.5 (d). This spectrum is generated with a cavity depth $e_c = 54$ mm, a relative bandwidth of 31 %, and $\alpha = 0.6$ around the central frequency $f_c = 509$ Hz. The plots in Fig. 5 clearly show that the trained model produces sound absorptions that are in good agreement with the simulated FEM responses. The correlation coefficients between the model and the FEM responses in these examples were greater than 0.99. **The proposed forward model resulted in a speed improvement of over four orders of magnitude compared to FEM simulation on a typical personal computer.**

5. Inverse design of membrane-type metasurface absorber

The membrane absorbers presented in this study are characterized by high and narrow absorption peaks at specific frequencies. Broader frequency absorption using these structures can be achieved through the coupling of the high-order elastic modes of the single membrane. These couplings occur with specific geometrical parameters of the membrane and the air cavity. They are, however, not easy to describe using simple analytical models. This section aims to illustrate the application of the proposed inverse design approach (Section 2.2) to realize absorbers with prominent absorption peaks at selected subwavelength frequencies and broadband absorbers. Subsection 5.1 describes the estimation of the membrane parameters for a given reference absorption profile, Subsection 5.2 discusses the fabrication process, and Subsection 5.3 presents the experimental protocol and the results.

5.1 Reference absorption profile and parameters estimation

Depending on the intended response of the absorber, a desired (reference) absorption profile \mathbf{r}^d should be first defined. The membrane parameters \mathbf{x}^* are then estimated by minimizing the deviation between the model output \mathbf{y} and \mathbf{r}^d using the inverse design approach (see Section 2.2). The algorithm remains the same, except that the error computation in Step 3 should include only the frequency range or the frequency values of interest. The algorithm starts from a random initial point \mathbf{x}^0 and produces a sequence of parameter estimates \mathbf{x}^k ($k = 0, 1, 2, \dots$) with the objective to minimize the cost function $E(\mathbf{x}) = \|\mathbf{r}^d - \mathbf{y}(\mathbf{x})\|^2$. Depending on the starting point (\mathbf{x}^0), the algorithm might converge to different local minima; this is due to the fact that different combination of parameters may yield similar values of the cost function. Different random initial values are evaluated, and the best fit is presented. In this section, three case studies are presented: single narrow-band, dual narrow-band, and wideband absorber. Here, we consider only the frequency range covered by the impedance tube (up to 1500 Hz).

- a) **Single narrow-band absorber.** One way to define the reference absorption profile \mathbf{r}^d is using the frequency response of a second-order resonator of the form:

$$H(s) = K \frac{s}{s^2 + \Delta\omega_p s + \omega_p^2}, \quad (8)$$

where K is a constant gain, $\Delta\omega_p$ represents the half-power (3 dB) bandwidth, and $\omega_p = 2\pi f_p$ is the peak or resonant frequency. The bandwidth is inversely proportional to the Q-factor Q_p , $\Delta\omega_p = \omega_p/Q_p$. Fig. 6 shows an example of a reference absorption spectrum (green dashed line) with absorption level $\alpha = 1$ at $f_p = 1,252$ Hz and Q-factor $Q_p = 32$, along with the estimated model (blue dotted line) and FEM responses (red solid line). The estimated parameters are summarized in Table 1. The estimated model response is highly correlated with the desired response around the peak frequency. It contains a second small peak at frequency $f = 624$. The estimated model response is then validated numerically using FEM simulation, and the two responses match very well.

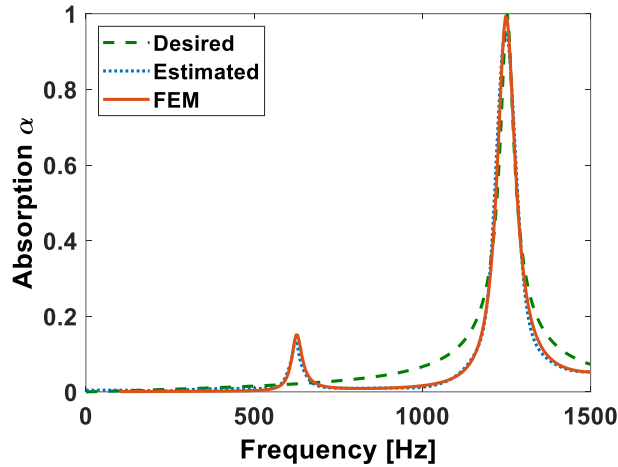


Fig. 6. Single narrow-band absorber: desired spectrum absorption profile (dashed), the estimated model response (dotted line) and FEM response (solid line)

- b) **Dual narrow-band absorber.** The reference response in this case can be defined as the desired absorption level (α) at specific frequencies f_1 and f_2 . Fig. 7 is an example of a reference response with absorption level $\alpha = 1$ at $f_1 = 540$ Hz and $f_2 = 889$ Hz. The estimated model response and the FEM simulation are also included. The estimated membrane parameters are summarized in Table 1. The inverse parameters estimation converges to α values equal to 0.99 at the selected frequencies. The predicted response, obtained using the estimated parameters, is very close to the response obtained with FEM simulation; the FEM response has a slightly lower absorption coefficient, $\alpha = 0.9$, at f_1 .

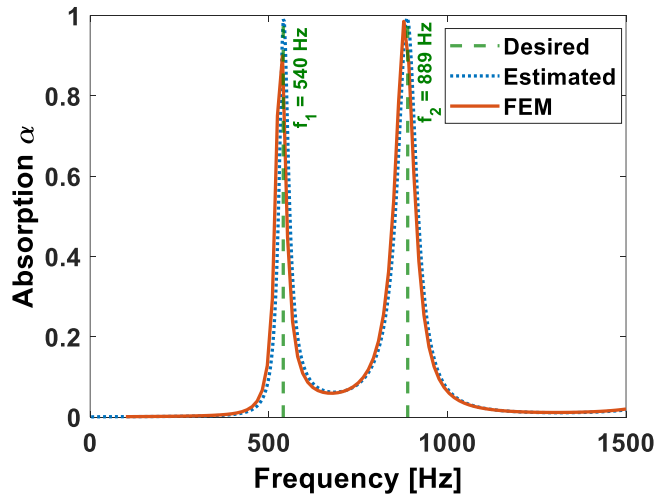


Fig. 7. Dual narrow-band absorber: desired spectrum absorption profile (dashed), the estimated model response (dotted line) and FEM response (solid line)

- c) **Wideband absorber.** The reference response in this case can be the desired absorption level (α) over the specific frequency band of interest. Fig. 8 is an illustration of a wideband reference response with a relative bandwidth of 23 % for $\alpha = 0.8$ around the central frequency $f_c = 975$ Hz. The estimated spectrum correlates well with the desired response in terms of general tendencies. The discrepancies between the two spectra are due to the constraints of the natural shape of the resonance of the membrane as well as the complexity of the desired response.

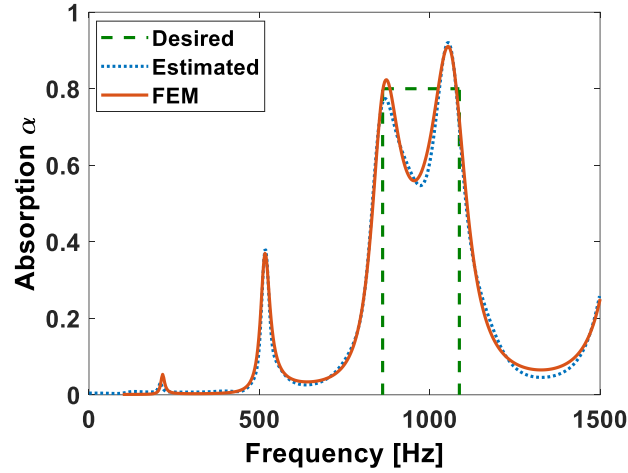


Fig. 8. Wideband absorber: desired spectrum absorption profile (dashed), the estimated model response (dotted line) and FEM response (solid line)

Table 1: Estimated membrane parameters

Estimated parameters	Simple absorber	Dual-band absorber	Wideband absorber
Radius a (mm)	25.5	24.7	30.9
Thickness h (mm)	0.0509	0.0500	0.0247
Cavity depth e_c (mm)	4.0	13.5	16.9

5.2 Fabrication of the membranes

Based on the finding of Section 5.1, we selected the single and the dual narrow band absorbers for fabrication. Each of these elasto-acoustic metasurfaces comprises a circular membrane backed by an air cavity with rigid endings. Each device is made up of two polymer cuboids with cylindrical cavities and a steel sheet membrane. The cuboids were created layer-by-layer using an additive manufacturing technique. For the first device, the first cuboid is of dimension 70x70x10 mm with a cylindrical cavity of radius $a = 25.5$ mm and a cavity depth $e_c = 4$ mm. The second cuboid has a dimension of 70x70x 5 mm with a cylindrical hollow air cavity of radius $a = 25.5$ mm. For the second device, the first cuboid is of dimension 70x70x10 mm with a cylindrical cavity of radius $a = 24.7$ mm and a cavity depth $e_c = 13.5$ mm. For both devices, a membrane of a side length of 70 mm and a thickness of 0.05 mm was sandwiched between the cuboids and secured using eight cap screws. The different parts of the membrane are illustrated in Fig.9.

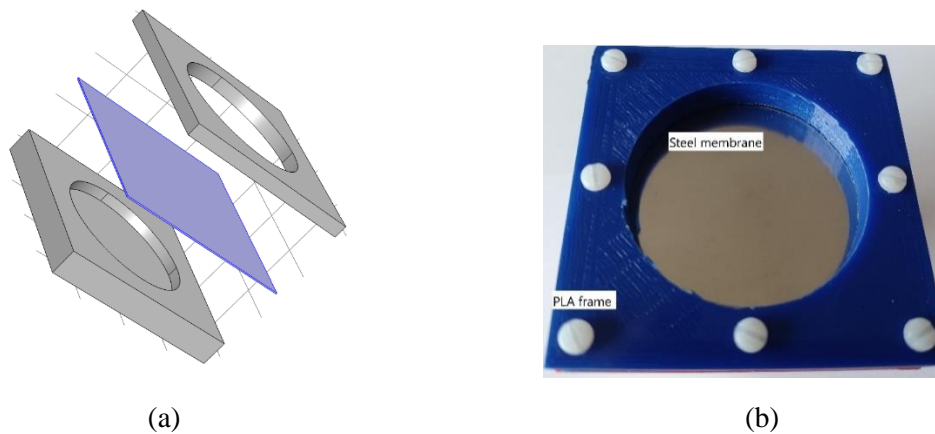


Fig.9. Example of sound absorber, (a) Schematic (b) Fabricated.

5.3 Experimental protocol and results

A non-commercial impedance tube apparatus based on the Two-Microphone transfer function method specified in the ISO 10534-2 protocol was used in this experiment, see Fig. 10. It serves at determining the complex reflection factor (R) and the dimensionless sound absorption coefficient (α) curve of the metasurface at different frequencies for normal sound incidence. The apparatus consists of a rigid rectangular impedance tube of inner cross section of 7x7 cm and length 60 cm, a loudspeaker mounted on one end of the tube, the metasurface membrane mounted at the other end and two identical microphones located on the side of the membrane to measure the acoustic pressure of the incident and reflected waves inside the tube. The two microphones are respectively located at 20 cm and 30 cm away from the surface of the structure. The loudspeaker generates broadband random signal covering the frequency range of interest namely, 50 to 1500 Hz. The pressure signals measured at the microphones are used to solve the pressure equation in the tube:

$$p(x) = p_0(e^{jkx} + Re^{-jkx}), \quad (9)$$

where p_0 is a constant; k is the wavenumber; the membrane is assumed to be at $x = 0$. The first and the second term in (9) represent respectively the incident and reflected waves.

By computing transfer function, ratio of pressures $H_{12} = \frac{p(x_2)}{p(x_1)}$, at the two microphone positions we can solve for the reflection factor ($R = \frac{H_{12}e^{jkx_1} - e^{jkx_2}}{e^{-jkx_2} - H_{12}e^{jkx_1}}$) and deduce the absorption coefficient as $\alpha = 1 - |R|^2$.

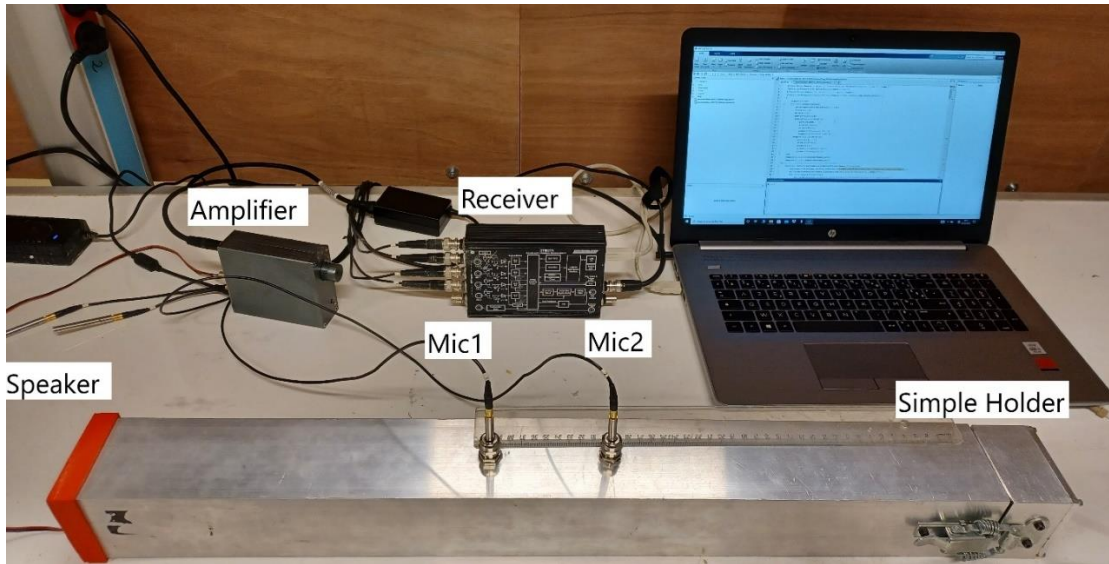


Fig 10. Experimental setup

The generated signals were amplified then processed using a multi-channel high-accuracy dynamic signal acquisition module connected to a computer for data analysis, Fig.9, depicts the results.

The experimental results show a good agreement with the estimated absorption spectrum ($\alpha_{FEM 1}$) in terms of general tendencies and spread around the peaking frequency. The main difference between the results in

the case of single narrow-band (Fig.9 a) is a shift in the frequency response of the experimental absorption curve towards the higher frequencies with a relative frequency shift of about 3 % and a 1.8 % decrease of the value of the resonance amplitude. Similar behavior was observed with the dual narrow-band absorber (Fig.9 b) with a slight difference in the shift between the first and second prominent peaks.

Replacing the COMSOL default value of the Young Modulus ($E = 200$ GPa) used in the first simulation (blue curve in Fig. 11) by the actual value ($E = 275$ GPa) of the reinforced stainless steel used in the experiment resulted in an upward shift in resonance frequencies ((red curve in Fig. 11) towards the experimental values. Other shifts and discrepancies are due to modeling errors caused by the deformation in the fabrication of the 3D-printed frame and the inaccuracies that occur during the assembly process. In the numerical model, we assumed rigid condition on the lateral boundaries of the membrane, which is very difficult to achieve experimentally. Practically, sandwiching and pressing the steel membrane between the rigid frame induces a static stress in the clamped boundary, which affects the mechanical vibration and results in a shift of the resonant frequency.

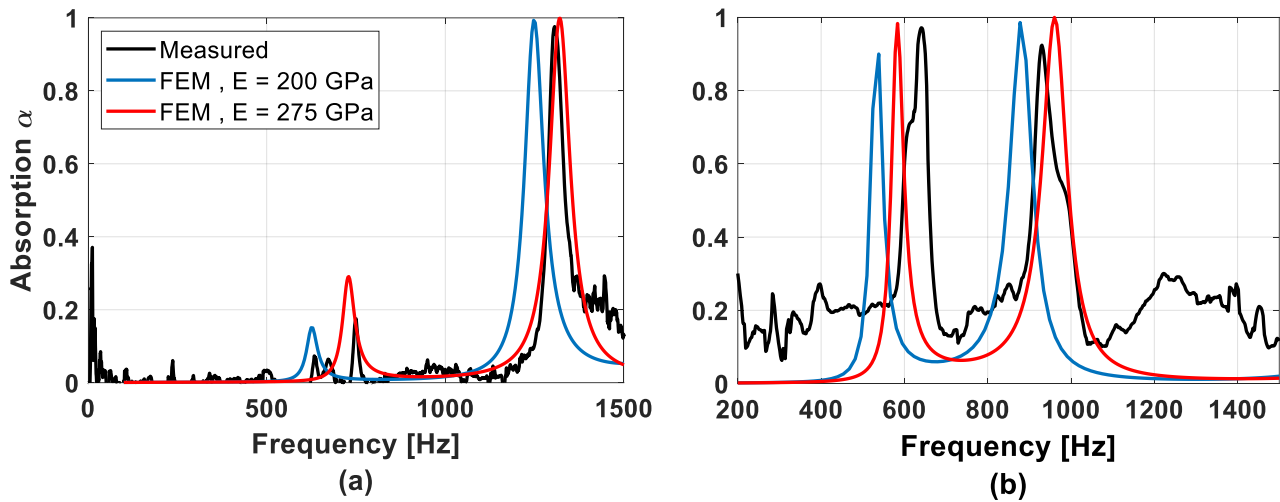


Fig 11. Measured and FEM simulated absorption spectrums with COMSOL default (blue curve) and actual (red curve) Young modulus, (a) single narrow band absorber, (b) dual narrow-band absorber

6 Conclusion

This study presented a systematic framework for the forward modeling and inverse design of membrane-type metasurfaces sound-absorbers. Once trained, the forward model reduces the computational time by orders of magnitude compared to conventional approaches. The iterative inversion method finds the input that reconstructs the desired output when cascaded with the forward model. We validated the proposed approach numerically and experimentally. This data-driven approach simplifies the way of designing metasurfaces with desired acoustic properties.

7 References

- [1] D. Smith, W. Padilla, D. Vier, S. Nemat-Nasser, and S. Schultz. Composite medium with simultaneously negative permeability and permittivity. *Physical review letters*, 84(18):4184– 4187, 2000
- [2] Bessa MA, Glowacki P, Houlder M. Bayesian machine learning in metamaterial design: Fragile becomes supercompressible. *Advanced Materials*. 2019 Nov;31(48):1904845.

- [3] Khatib O, Ren S, Malof J, Padilla WJ. Deep Learning the Electromagnetic Properties of Metamaterials—A Comprehensive Review. *Advanced Functional Materials*. 2021 May 28;2101748.
- [4] Assouar B, Liang B, Wu Y, Li Y, Cheng JC, Jing Y. Acoustic metasurfaces. *Nature Reviews Materials*. 2018 Dec;3(12):460-72.
- [5] Jie Zhu, Xuefeng Zhu, Xiaobo Yin, Yuan Wang, and Xiang Zhang. Unidirectional Extraordinary Sound Transmission with Mode-Selective Resonant Materials. *Phys. Rev. Applied* 13, 041001 (2020).
- [6] Park JJ, Park CM, Lee KJ, Lee SH. Acoustic superlens using membrane-based metamaterials. *Applied Physics Letters*. 2015 Feb 2;106(5):051901.
- [7] Z. Liu, X. Zhang, Y. Mao, Y. Y. Zhu, Z. Yang, C. T. Chan, and P. Sheng, “Locally resonant sonic materials,” *Science* 289(5485), 1734–1736 (2000)
- [8] Jie Zhu, Xuefeng Zhu, Xiaobo Yin, Yuan Wang, and Xiang Zhang. Unidirectional Extraordinary Sound Transmission with Mode-Selective Resonant Materials. *Phys. Rev. Applied* 13, 041001 (2020).
- [9] Park JJ, K. J. B. Lee, Oliver B. Wright, Myoung Ki Jung, and Sam H. Lee. Giant Acoustic Concentration by Extraordinary Transmission in Zero-Mass Metamaterials. *Phys. Rev. Lett.* 110, 244302 – Published 13 June 2013
- [10] Z. Liu, X. Zhang, Y. Mao, Y. Y. Zhu, Z. Yang, C. T. Chan, and P. Sheng, “Locally resonant sonic materials,” *Science* 289(5485), 1734–1736 (2000)
- [11] A. Elayoucha), M. Addouche, and A. Khelif. Extensive tailorability of sound absorption using acoustic metamaterials. *Journal of Applied Physics* 124, 155103 (2018)
- [12] F Capolino, M Khajavikhan, A Alù, Metastructures: From physics to application. *Applied Physics Letters* 120 (6), 060401 (2022)
- [13] Sichao Qu and Ping Sheng. Minimizing Indoor Sound Energy with Tunable Metamaterial Surfaces. *Phys. Rev. Applied* 14, 034060 – Published 23 September 2020
- [14] J Li, X Wen, P Sheng, Acoustic metamaterials, *Journal of Applied Physics* 129 (17), 171103 (2021)
- [15] M Yang, S Chen, C Fu, P Sheng, Optimal sound-absorbing structures, *Materials Horizons* 4 (4), 673-680 (2017).
- [16] Y Li, BM Assouar. Acoustic metasurface-based perfect absorber with deep subwavelength thickness. *Applied Physics Letters* 108 (6), 063502
- [17] H Eshfahani, Y Mazor, A Alù. Homogenization and design of acoustic Willis metasurfaces. *Physical Review B* 103 (5), 054306 (2021).
- [18] Lan, J., Li, Y., Xu, Y. *et al.* Manipulation of acoustic wavefront by gradient metasurface based on Helmholtz Resonators. *Sci Rep* 7, 10587 (2017). <https://doi.org/10.1038/s41598-017-10781-5>
- [19] B.H. Song and J.S. Bolton. A transfer-matrix approach for estimating the characteristic impedance and wave numbers of limp and rigid porous materials. *J. Acoust. Soc. Am.* 107(3), pp. 1131-1152 (1999).
- [20] N. Jiménez, V. Romero-García, A. Cebrecos, R. Picó, V.J. Sánchez-Morcillo and L.M. Garcia-Ra. Broadband quasi perfect absorption using chirped multi-layer porous materials. *AIP Advances*, 6, 121605 (2016)
- [21] D. Li, D. Chang and B. Liu. Enhanced low to mid-frequency sound absorption using parallel arranged perforated plates with extended tubes and porous material. *Applied Acoustics*, 127, pp. 316-323 (2017)
- [22] Li J, Hesthaven JS. Analysis and application of the nodal discontinuous Galerkin method for wave propagation in metamaterials. *Journal of Computational Physics*. 2014 Feb 1;258:915-30.
- [23] Donda K, Zhu Y, Merkel A, Fan SW, Cao L, Wan S, Assouar B. Ultrathin acoustic absorbing metasurface based on deep learning approach. *Smart Materials and Structures*. 2021 Jun 18;30(8):085003.
- [24] Liu L, Xie LX, Huang W, Zhang XJ, Lu MH, Chen YF. Broadband acoustic absorbing metamaterial via deep learning approach. *Applied Physics Letters*. 2022 Jun 20;120(25):251701.

- [25] Alguacil A, Bauerheim M, Jacob MC, Moreau S. Predicting the propagation of acoustic waves using deep convolutional neural networks. *Journal of Sound and Vibration*. 2021 Nov 10;512:116285.
- [26] Zhang H, Wang Y, Lu K, Zhao H, Yu D, Wen J. SAP-Net: Deep learning to predict sound absorption performance of metaporous materials. *Materials & Design*. 2021 Dec 15;212:110156.
- [27] Kumar S, Tan S, Zheng L, Kochmann DM. Inverse-designed spinodoid metamaterials. *npj Computational Materials*. 2020 Jun 5;6(1):1-0.
- [28] Krupali Donda, Yifan Zhu, Aurélien Merkel, Shi-Wang Fan, Liyun Cao, et al.. Ultrathin acoustic absorbing metasurface based on deep learning approach. *Smart Materials and Structures*, IOP Publishing, 2021, 30 (8), pp.085003. [ff10.1088/1361-665X/ac0675f](https://doi.org/10.1088/1361-665X/ac0675f)
- [29] Bessa MA, Glowacki P, Houlder M. Bayesian machine learning in metamaterial design: Fragile becomes supercompressible. *Advanced Materials*. 2019 Nov;31(48):1904845.
- [30] Khatib O, Ren S, Malof J, Padilla WJ. Deep learning the electromagnetic properties of metamaterials—a comprehensive review. *Advanced Functional Materials*. 2021 Aug;31(31):2101748.
- [31] Lu BL, Kita H, Nishikawa Y. Inverting feedforward neural networks using linear and nonlinear programming. *IEEE Transactions on Neural networks*. 1999 Nov;10(6):1271-90.
- [32] Kindermann J, Linden A. Inversion of neural networks by gradient descent. *Parallel computing*. 1990 Aug 1;14(3):277-86.
- [33] Jordan MI, Rumelhart DE. Forward models: Supervised learning with a distal teacher. *Cognitive science*. 1992 Jul 1;16(3):307-54.
- [34] Peurifoy J, Shen Y, Jing L, Yang Y, Cano-Renteria F, DeLacy BG, Joannopoulos JD, Tegmark M, Soljačić M. Nanophotonic particle simulation and inverse design using artificial neural networks. *Science advances*. 2018 Jun 1;4(6):eaar4206.
- [35] Liu D, Tan Y, Khoram E, Yu Z. Training deep neural networks for the inverse design of nanophotonic structures. *Acs Photonics*. 2018 Feb 25;5(4):1365-9.
- [36] Ma W, Liu Z, Kudyshev ZA, Boltasseva A, Cai W, Liu Y. Deep learning for the design of photonic structures. *Nature Photonics*. 2021 Feb;15(2):77-90.
- [37] He L, Guo H, Jin Y, Zhuang X, Rabczuk T, Li Y. Machine-learning-driven on-demand design of phononic beams. *Science China Physics, Mechanics & Astronomy*. 2022 Jan;65(1):214612.
- [38] Ding H, Fang X, Jia B, Wang N, Cheng Q, Li Y. Deep learning enables accurate sound redistribution via nonlocal metasurfaces. *Physical Review Applied*. 2021 Dec 14;16(6):064035.
- [39] Wong E, Kolter JZ. Neural network inversion beyond gradient descent. *OPTML 2017: 10th NIPS Workshop on Optimization for Machine Learning (NIPS 2017)*
- [40] Jensen CA, Reed RD, Marks RJ, El-Sharkawi MA, Jung JB, Miyamoto RT, Anderson GM, Eggen CJ. Inversion of feedforward neural networks: algorithms and applications. *Proceedings of the IEEE*. 1999 Sep;87(9):1536-49.
- [41] Raymond SJ, Collins DJ, O’Rourke R, Tayebi M, Ai Y, Williams J. A deep learning approach for designed diffraction-based acoustic patterning in microchannels. *Scientific reports*. 2020 May 26;10(1):8745.

Data availability: The data that support the findings of this study are available from the corresponding author upon reasonable request.

Code availability: The code used for this study are available from the corresponding author upon reasonable request.